MID-AMERICA TRANSPORTATION CENTER

Report # MATC-MS&T: 139-1

Final Report
WBS: 25-1121-0005-139-1

Investigation of Wind Effects on Bridges Induced by Tornados for Tornado-Resistant Design - Phase I

Grace Yan, PhD
Associate Professor
Department of Civil, Architectural, and Environmental Engineering
Missouri University of Science & Technology

Zhi Li
PhD Candidate

2020

A Cooperative Research Project sponsored by
U.S. Department of Transportation- Office of the Assistant Secretary for Research and Technology

MATC

Investigation of Wind Effects on Bridges Induced by Tornadoes for Tornado-Resistance Design - Phase I

Final Report

Grace Yan, PhD
Associate Professor
Department of Civil, Architectural and Environmental Engineering
Missouri University of Science and Technology

Zhi Li
PhD Candidate
Department of Civil, Architectural and Environmental Engineering
Missouri University of Science and Technology

A Report on Research Sponsored by

Mid-America Transportation Center

University of Nebraska–Lincoln

September 2020

Technical Report Documentation Page

1. Report No. 25-1121-0005-139-1	2. Government Accession No.	3. Recipient's Catalog No.
4. Title and Subtitle Investigation of Wind Effects on Bridges Induced by Tornadoes for Tornado-Resistance Design – Phase I		5. Report Date Sept. 15, 2020
		6. Performing Organization Code
7. Author(s) Guirong Yan and Zhi Li		8. Performing Organization Report No. 25-1121-0005-139-1
9. Performing Organization Name and Address Mid-America Transportation Center Prem S. Paul Research Center at Whittier School 2200 Vine St. Lincoln, NE 68583-0851		10. Work Unit No. (TRAIS)
		11. Contract or Grant No. 69A3551747107
12. Sponsoring Agency Name and Address Office of the Assistant Secretary for Research and Technology 1200 New Jersey Ave., SE Washington, D.C. 20590		13. Type of Report and Period Covered January 2019-June 2020
		14. Sponsoring Agency Code MATC TRB RiP No. 91994-42
15. Supplementary Notes		

16. Abstract
The impact of tornadoes on civil structures is often devastating and results in loss of property, injury of human beings and/or loss of lives. Thirteen bridges were destroyed or severely damaged by tornadoes in the USA in the past. Even in the latest version of the AASHTO Bridge Design Specifications (8th Edition 2017), no specifications on design tornadic wind loads have been included. To prevent bridges from being severely damaged or destroyed during future tornado incidents, it is imperative to characterize the wind effects induced by tornadoes on bridges and determine the design tornadic wind loads for bridges. This project characterized the wind effects of tornadoes on bridges using computational fluid dynamics (CFD) simulations, and modified the equations for calculating the design wind pressure on bridges. The obtained research findings will facilitate the tornado-resistance design of new bridges and the reinforcement of existing bridges to be tornado resistant. This will eventually prevent bridges from failure during tornado incidents to enhance the safety of highway or railroad bridges.

17. ORCID No. of each Researcher Gurong (Grace) Yan ORCID: 0000-0001-6950-7692	18. Distribution Statement		
19. Security Classif. (of this report) Unclassified	20. Security Classif. (of this page) Unclassified	21. No. of Pages 30	22. Price

Table of Contents

List of Figures

Disclaimer

The contents of this report reflect the views of the authors, who are responsible for the facts and the accuracy of the information presented herein. This document is disseminated in the interest of information exchange. The report is funded, partially or entirely, by a grant from the U.S. Department of Transportation's University Transportation Centers Program. However, the U.S. Government assumes no liability for the contents or use thereof.

Abstract

The impact of tornadoes on civil structures is often devastating and results in loss of property, injury of human beings and/or loss of lives. Thirteen bridges were destroyed or severely damaged by tornadoes in the USA in the past. Even in the latest version of the AASHTO Bridge Design Specifications (8th Edition 2017), no specifications on design tornadic wind loads have been included. To prevent bridges from being severely damaged or destroyed during future tornado incidents, it is imperative to characterize the wind effects induced by tornadoes on bridges and determine the design tornadic wind loads for bridges. This project characterized the wind effects of tornadoes on bridges using computational fluid dynamics (CFD) simulations, and modified the equations for calculating the design wind pressure on bridges. The obtained research findings will facilitate the tornado-resistance design of new bridges and the reinforcement of existing bridges to be tornado resistant. This will eventually prevent bridges from failure during tornado incidents to enhance the safety of highway or railroad bridges.

Chapter 1 Research Motivation and Research Objective

1.1 Research Motivation

In recent years, tornadoes (see fig. 1.1) have become a significant cause of injury, death, and property damage in the US. They are causing an average of $10B of economic loss each year. In 2011 only, the tornado-induced property loss exceeded $20B and 550 people were killed [1,2]. For example, on May 22, 2011, an EF5 tornado struck Joplin, MO. It killed 161 people, injured more than 1000 and caused $2.8B of property damage. To reduce the tornado-induced loss, it is imperative to develop a tornado resistant design. For buildings, no matter whether it is residential or commercial, the idea of implementing a tornado-resistant design has been widely accepted. Although a tornado resign design for normal buildings is not required in the current wind design practice (ASCE 7-16), in the next version of ASCE 7 (ASCE7- 22), a tornado resistant design will be required. In ASCE 7-22, a new chapter, which is chapter 32, will be added to provide the specification of a tornado resistant design for buildings.

For bridges, the wind design is governed by AASHTO, Section 3.8 Wind load. This research seeks to answer the question whether or not a tornado resistant design should be enforced for bridges. The answer depends on whether tornadoes have destroyed any bridges. Unfortunately, the answer is “yes”. Thirteen bridges were destroyed or severely damaged by tornadoes in the USA in the past (see fig. 1.2-1.5). For example, the railroad bridge crossing the Kinzua gorge was completely destroyed by a low-intensity tornado (ranked as F-1) on July 21, 2003 (Leech, 2005) [3]. Eleven of its 20 towers were taken down, as shown in figure 1.2. At that time, the wind speed was just 73-112 mph. The fact that the bridge was destroyed at such a low wind speed suggests the wind effects of tornadoes (swirling, rotating winds) are completely

different from those induced by straight-line winds. Therefore, it is imperative to study the wind effects of tornadoes on bridges and develop a tornado-resistant design code for bridges.

Figure 1.1 A tornado

Figure 1.2 Kinzua bridge (F1 tornado in 2003)

Figure 1.3 Utica Swing Bridge, 1906

Figure 1.4 New Castle Bridge, 2013

Figure 1.5 Hurricane Creek Bridge, 2011, F4

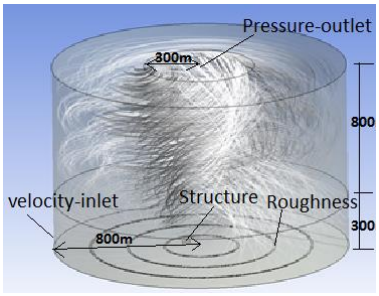

Figure 1.6 Simulated tornadic wind field

1.2 Research Objective

Through a comprehensive literature review, the wind effects induced by tornadoes on bridges have not been studied yet, although a lot of research has been conducted on the tornadic wind effects of other types of civil structures [4,5,6,7,8,9,10,11,12,13,14,15,16]. To avoid catastrophic failure of bridges under tornadoes, the objective of this study is to investigate the wind effects of tornadoes on bridges and improve the wind design of bridges to resist tornadoes. To achieve this research objective, we not only need to simulate tornadic wind field and

investigate the wind effects of tornadoes on bridges, but also need to simulate equivalent straight-line wind field and obtain the wind effects of straight-line winds on bridges. This is because the current wind design in AASHTO is based on straight-line winds. The obtained research findings will be used to determine the design tornadic wind loads for bridges.

1.3 Description of the Bridge of Interest

In this study, a newly designed bridge on Highway 32 over Cedar Creek west of Stockton in Missouri, which will replace the existing bridge (see fig. 1.7), is considered. The information of the new bridge is shared by MODoT, as shown in figure 1.8. The estimated total cost is $4 million. It is expected that approximately 1,900 vehicles cross this bridge per day. This is a girder bridge with three spans, made of pre-stressed concrete. It is 300 ft long, with the main span of 120 ft. It is 32 ft wide and holds two traffic lanes.

Figure 1.7 The existing bridge which needs to be replaced

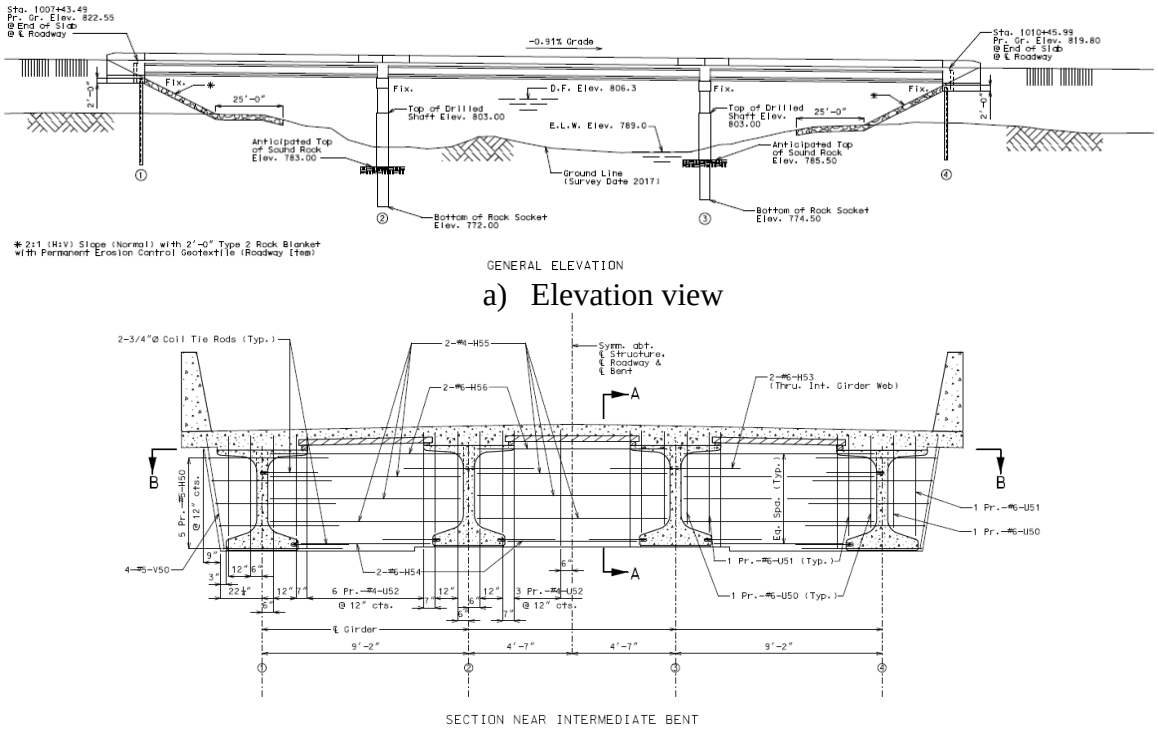

a) Elevation view

b) Cross section

Figure 1.8 The new bridge on Highway 32 over Cedar Creek west of Stockton in Missouri

1.4 Research Tasks

To achieve the stated research objective, the following three research tasks have been conducted. First, simulate tornadoes and characterize tornadic wind effects on a girder bridge, as detailed in Chapter 2; Second, characterize the wind effects under equivalent straight-line winds and compare the wind effects between tornadic winds and the equivalent straight-line winds, as detailed in Chapter 3; Third, modify the equation to calculate the design wind pressure in AASHTO code, as detailed in Chapter 4; and Fourth, conclusions and future work are presented in Chapter 5. In this project, Computational Fluid Dynamics (CFD) simulation will be applied to simulate the 3D tornadic wind field and its equivalent straight-line winds, and to investigate the wind pressure on bridges induced by different winds.

Chapter 2 Simulation of Tornadic Wind Field and Investigation of Wind Effects of Tornadoes on Bridges

In this chapter, a real-world tornado, the Spencer, SD Tornado of 30 May 1988, is simulated at a full-scale using CFD simulations and the wind effects of this tornado on a girder bridge are characterized. Two numerical models will be developed. The first one does not include the bridge in the computational domain. This is to validate the efficacy of the tornadic wind field simulation. The second model is to include the bridge of interest in the computational domain. That is, a full-scale tornadic wind field with a full-scale short-span girder bridge present will be simulated. This is to find the wind pressure on bridge surface and total forces/moments induced by tornadoes.

2.1 CFD Simulation Setup

To simulate a tornadic wind field in which the air flow swirls, a cylindrical computational domain is applied, as shown in figure 2.1. It is a full-scale simulation. The height of the velocity inlet is 100 m and the radius of the pressure outlet is 340 m. In this computational domain, the inflow surface boundary condition is velocity-inlet, and the outflow surface boundary condition is pressure-outlet. All other boundary surfaces are no-slip walls. To accurately capture the tornadic flow field and quantitatively investigate the wind loading on the structure, in the central part of the convergent zone and the vicinity near the ground, a fine mesh is applied.

The CFD simulation is based on Large Eddy Simulation, which is governed by filtered time-dependent Navier-Stokes equations. Assuming that momentum and mass are mainly transported by large eddies, the large eddy simulation (LES) with Dynamic Smagorinsky-Lilly subgrid model is adopted for turbulence modeling to capture the characteristics of multiple vortices. The segregated implicit solver is used to solve the governing equation with a SIMPLEC

(Smei-Implicit Method for Pressure Linked Equation) method is used for Pressure-velocity Coupling, as the SIMPLEC scheme usually has a better convergence than PISO (Pressure–Implicit with Splitting of Operators) [17].

To generate a stationary tornadic wind field, the simulation is run for 260 s at first. To simulate the translation of the tornado, a relative motion is established between the bridge and the ground surface of the computational domain, by moving the bridge on the opposite direction, at the same speed as tornado translation, which is 15 m/s here. The Layering technique is applied as the dynamic meshing method and another 48 s is run for simulating the translation of the tornado. The time step of the simulation is 0.01 s. The total number of cells is approximately 1.4 million.

2.2 Velocity Input

The velocity input at the velocity inlet are defined in equations 2.1, 2.2 and 2.3. They are the tangential velocity profile along height and the radial velocity profile along height, which are the regression equations of the radar-measured velocity data at the radius of 800 m of the Spencer, SD tornado of 30 May 1988 [18]. All other boundary conditions are defined as symmetry.

$$\text{Tangential velocity: } V_t = 20.61(Z/20)^{0.1774} \tag{2.1}$$

$$\text{Radial velocity: } V_r = -31.34\left(\frac{Z}{20}\right)^{0.169} \qquad Z \le 20\ m \tag{2.2}$$

$$V_r = 45.14\left(\frac{Z}{20}\right)^{0.1826} - 76.48 \qquad Z \ge 20\ m \tag{2.3}$$

where Z is the height from the ground surface.

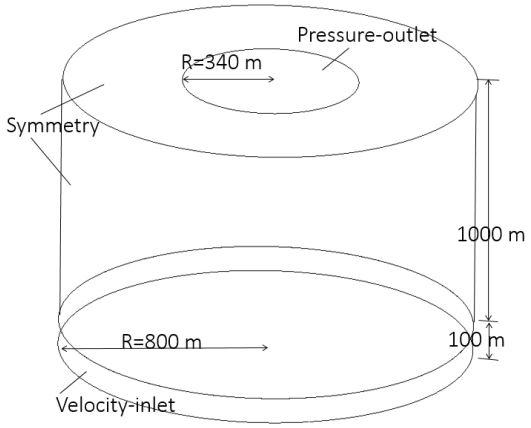

Figure 2.1 Computational domain of the tornadic wind field

2.3 Validation of the simulated tornadic wind field

The radar-measured velocity data will be used to validate the efficacy of the simulation strategies. The tangential velocity profile along the radius at the elevation of 80 m is extracted and presented in figure 2.2, as shown in the red graph. The tangential velocity is time-averaged for the period of 260 s to 300 s. To validate the simulation, the instantaneous tangential velocity profile extracted from the radar-measured velocity data of the Spencer, SD tornado of 30 May 1988, is also presented in figure 2.2, as shown in the black graph. These two graphs match each other reasonably well in terms of the maximum tangential velocity and the core radius, validating the numerical simulation of the tornadic wind field.

Figure 2.3 presents the instantaneous tangential velocity distribution on the horizontal plane of 80 m at 270 s. The color represents the magnitude of tangential velocity and the arrows represent the direction of the resultant velocity of tangential and radial components. Outside the core region, the wind flow converges towards the tornado center, with increasing tangential velocity. Then, the tangential velocity reaches its maximum value at a certain radius, which is called the core radius, before decreasing along the radial distance from the core radius to the tornado center.

In general, circular strips are formed, and the velocity in each strip is uniform, while the tangential velocity in the core region is not that uniform, which may be because the relatively low rotational velocity cannot sustain in relatively high turbulence in the core region. Figure 2.3 shows that this tornado has a single vortex. Figure 2.4 presents the instantaneous tangential velocity distribution on a vertical plane through the tornado center. The color represents the magnitude of tangential velocity and the arrows represent the direction of the resultant velocity of radial and vertical components. A downdraft is observed at the center and updrafts are observed in the surrounding areas. These suggest that the flow structure is double-celled.

Figure 2.5 presents the instantaneous pressure contour on the horizontal plane at the elevation of 80 m. Regular circular strips are observed. The pressure gradually decreases along the radius from the outer edge to tornado center, which explains why the air outside the core region flows inwards while the air inside the core region flows outwards. Figure 2.6 presents the instantaneous pressure contour on the vertical plane through tornado center. Similarly, the pressure gradually decreases from the outer edge to the core region.

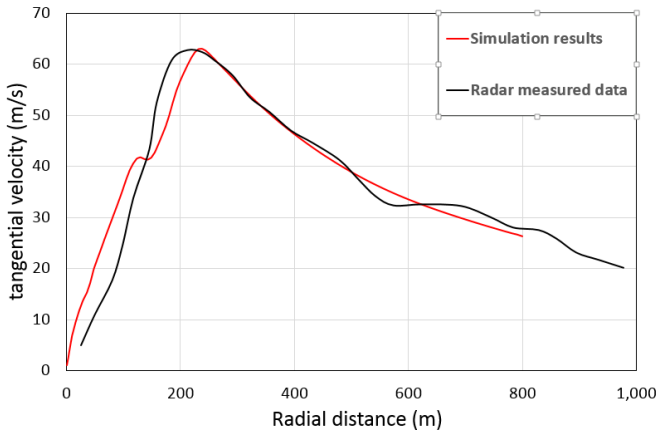

Figure 2.2 Tangential velocity along a line in radial distance at the elevation of 80 m

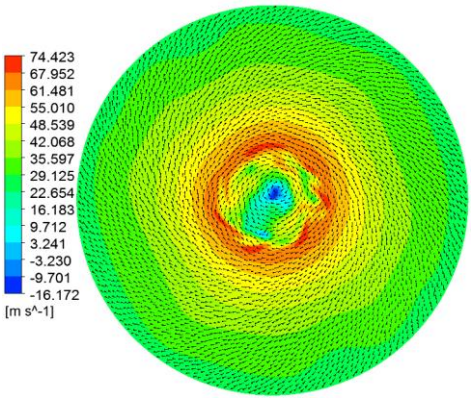

Figure 2.3 Instantaneous Tangential velocity distribution on the horizontal plane at the elevation of 80 m

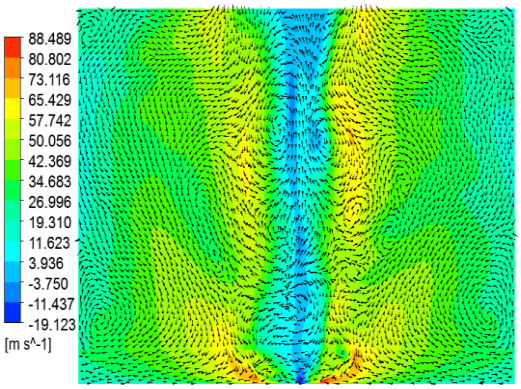

Figure 2.4 Instantaneous Tangential velocity on a vertical plane through tornado center

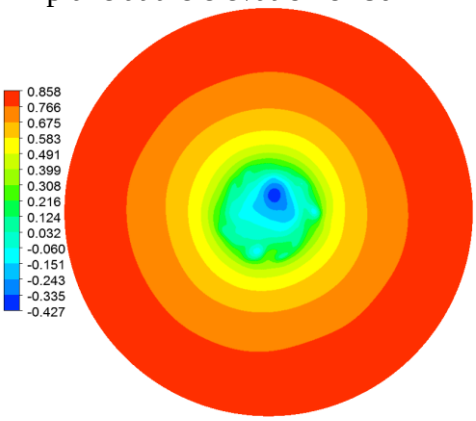

Figure 2.5 Instantaneous Pressure distribution on the horizontal plane at the elevation of 80 m

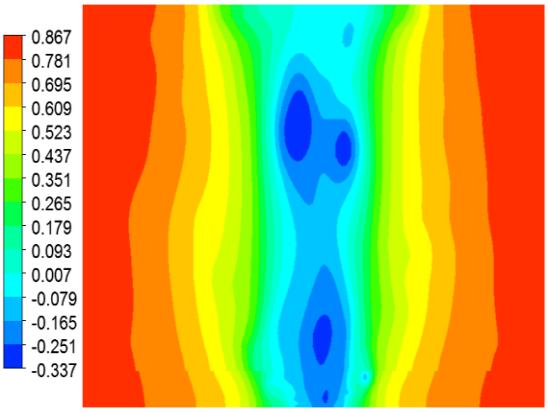

Figure 2.6 Instantaneous Pressure distribution on a vertical plane throuth tornado center

2.4 Wind Effects Induced by Tornadoes on Bridges

To obtain the wind effects on the bridge, the bridge is included in the tornadic wind field (see fig. 2.7). The pressure coefficient is adopted to represent the pressure distribution on the bridge surface. In this study, the pressure coefficient is calculated based on equation 2.4

$$C_p = \frac{P - P_r}{\frac{1}{2}\rho_r V_r^2} \tag{2.4}$$

where $P - P_r$ denotes the relative static pressure at the point where the pressure coefficient is evaluated. P_r, V_r, and ρ_r denote the reference pressure, reference wind velocity and air density,

respectively, which are $P_r = 101{,}325$ Pa, $V_r = 80.7$ m/s and $\rho_r = 1.225$ kg/m^3 in this study [18].

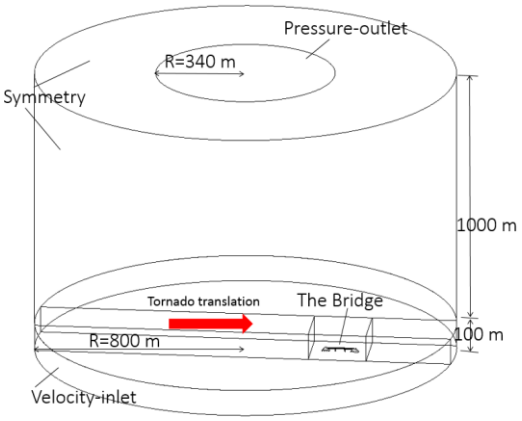

a) Tornadic wind field with the bridge included

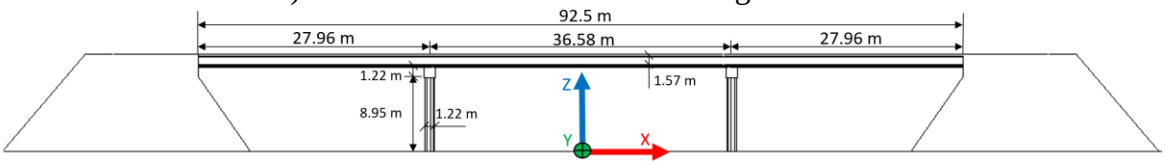

b) The dimentions of the bridge model in the computational domain

Figure 2.7 Computational domains for simulated cases

The pressure distribution on the bridge surface induced by the tornado is extracted at two representative time instants and presented in figure 2.8 and 2.9. The first time instant is associated with the time when the maximum positive pressure is observed. The location of the bridge in the computational domain is 360 m away from the center of the tornado, which is illustrated by figure 2.8a). The zoom-in figure of the region including bridge in figure 2.8a) is shown in Figure 2.8b), which clearly shows the streamlines in the tornadic wind field around the bridge. Figure 2.8c) presents the pressure coefficient on the bridge surface. Except a corner, the pressure on the bridge surface is dominated by positive pressure. This is because the bridge is located in the outer region of the computational domain at this time, where the positive pressure dominates the wind field and the blockage of the bridge to the wind flow does not distort the

streamline significantly. The peak value of the positive pressure coefficient is 1.4, which occurs on the windward side.

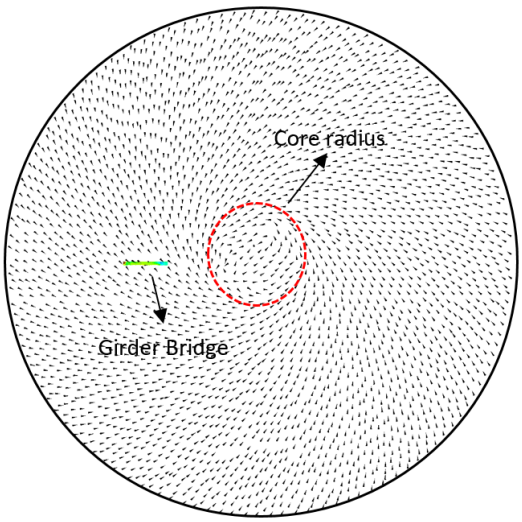

a) Location of the bridge

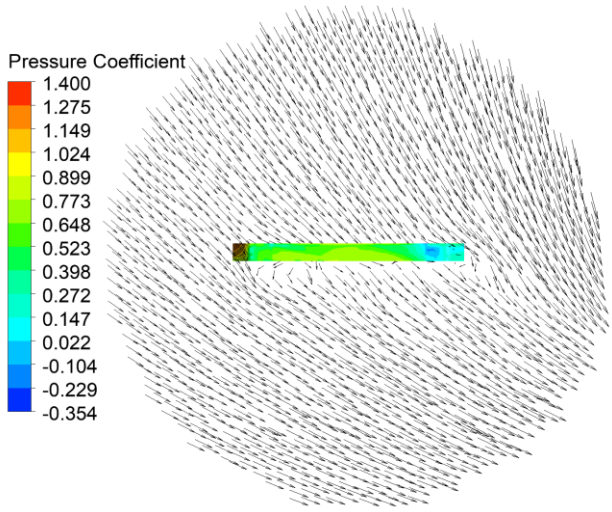

b) Streamline around the bridge

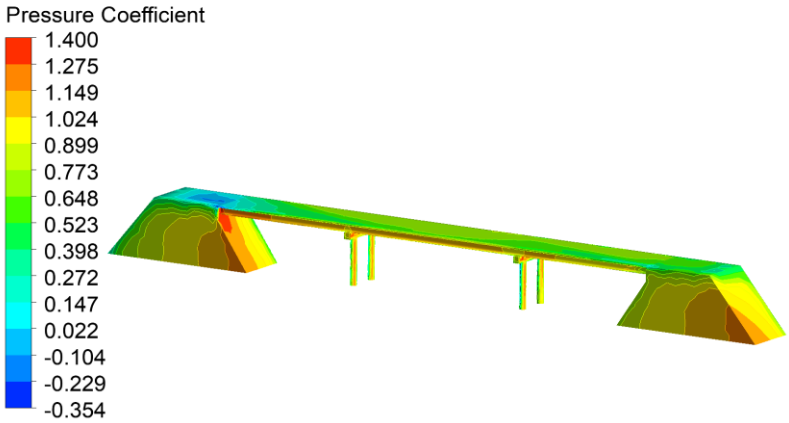

c) Pressure distribution on the bridge surface

Figure 2.8 Pressure distribution on bridge surface when the maximum positive pressure on the bridge surface is observed

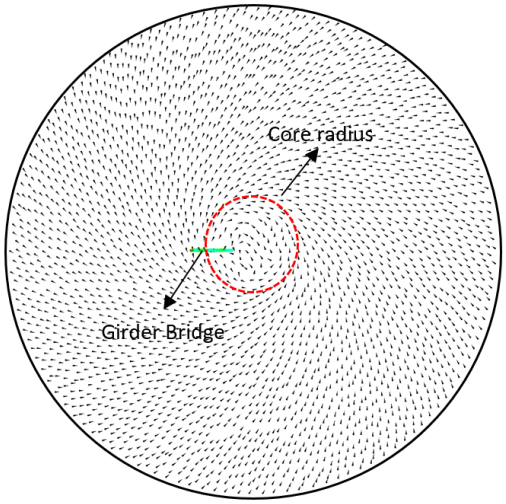

a) Location of the bridge

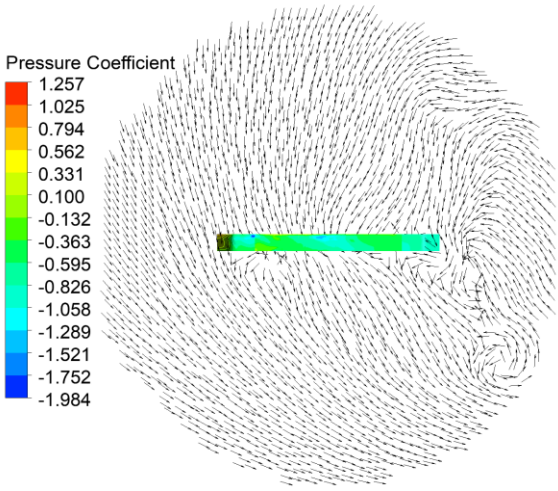

b) Streamline around the bridge

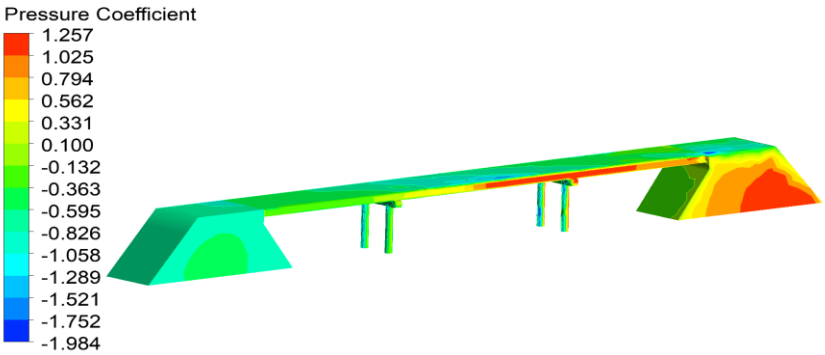

c) Pressure distribution on the bridge surface

Figure 2.9 Pressure distribution on bridge surface when the maximum negative pressure on the bridge surface is observed

In addition, the pressure distribution on the bridge surface when the maximum negative pressure is observed is also presented, as shown in figure 2.9. Figure 2.9a) presents the location of the bridge in the computational domain at this time instant, which is 135 m away from the center of the tornado. Figure 2.9b) presents the zoom-in figure of the region including the bridge in figure 2.9a), which shows the streamlines in the tornadic wind field around the bridge. At this time, the pressure on the bridge is dominated by the negative pressure. Two facts contribute to this. First, the bridge is located in the core region of the tornado, which is dominated by negative pressure due to atmospheric pressure drop; and second, the blockage of this bridge to the wind

flow may significantly alter the wind velocity, causing the air flow to accelerate when passing the bridge, which further decreases the pressure around the bridge, based on the Bernoulli Equation. The peak value of the negative pressure coefficient is -1.98, which occurs on the two sides of the piers.

2.5 Force and moment coefficients acting on the unit length of bridge deck induced by tornadic winds

To investigate the force and moment coefficients on the unit length (1 m) of the bridge deck, ANSYS mechanical 17.1 is applied to conduct the related structural analysis. First, the finite element model (FEM) of the unit length of bridge deck in the middle of the bridge is constructed by applying the DesignModeler in the workbench, as shown in figure 2.10. Then, the tornadic wind pressure on the bridge deck during the last 48s of simulation period (while the bridge moves) obtained from the CFD simulation is mapped onto this FEM by using the transient load mapping technique (ANSYS 2013), as shown in figure 2.11. Meanwhile, in order to obtain the force and the moment exerted on this FEM induced by the tornadic wind pressure, the fixed support boundary conditions are adopted on the two sides of this FEM, as shown in figure 12. Finally, the total force and moment coefficients acting on this unit length of the bridge deck are extracted.

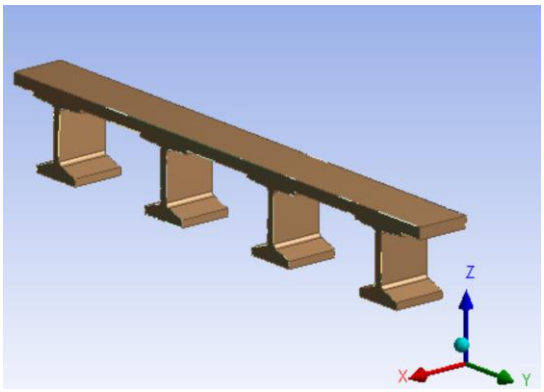

Figure 2.10 The FEM of the unit length of bridge deck

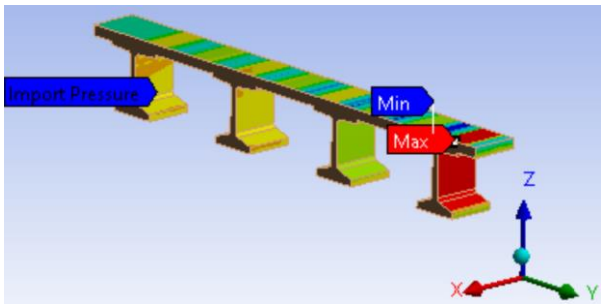

Figure 2.11 The FEM after importing the tornadic wind pressure onto the surface

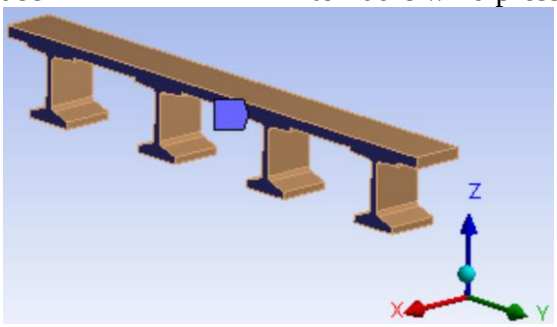

Figure 2.12 The FEM after adopting fixed support at two sides

From figure 2.13a), the force coefficient in the X direction (hereafter "Fx") is very small. In fact, no pressure is mapped onto the surface perpendicular to the X direction and fixed supports are applied on these two sides. The time history of the force coefficients in the Y and Z directions (hereafter "Fy" and "Fz") exhibit the trend that is similar to that acting on the entire bridge, as shall be shown in next chapter. Two peak values are observed when t=15s and 35s, which are the two time instants when the two core radii of the tornado approaches the bridge sequentially. And the lowest value can be observed when t=25 s, which is the time instant when the bridge is located at tornado center.

The time history of the moment coefficients is extracted and presented in figure 2.14. The moment coefficient about the X axis (hereafter "Mx"), as shown in figure 2.14a), and about the y axis (hereafter "My"), as shown in figure 2.14b), reveal the loading changes on the structure

when the tornado passes the bridge. There exist two peak values in the time history of Mx and My, which are associated with t=15s and 35s; and the smallest value occurs when t=25 s. The phenomena can be explained by the fact that Mx is calculated based on Fy and My is calculated based on Fz. That is to say, the change in Mx and My are related to the changes in Fy and Fz. However, Mz is calculated based on Fx, so its magnitude exhibits very slight changes through the time history.

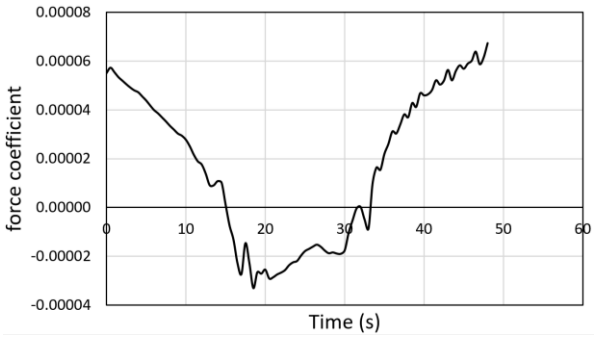

a) force coefficient in X direction

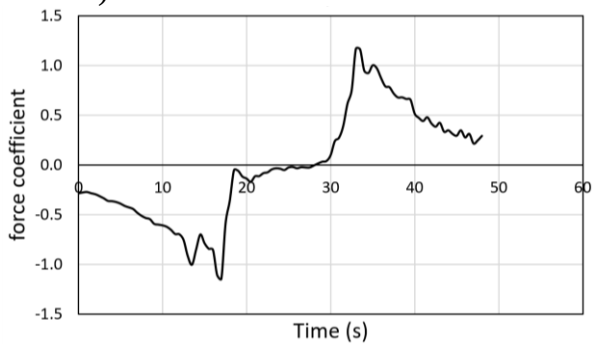

b) force coefficient in Y direction

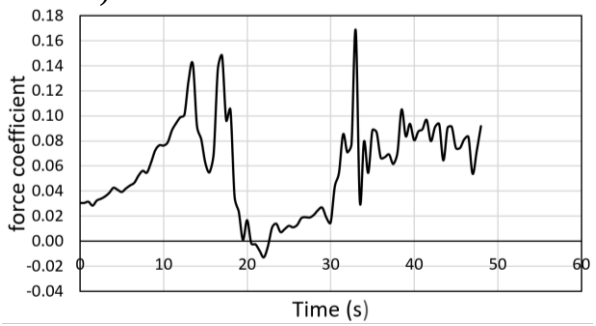

c) force coefficient in Z direction

Figure 2.13 Time history of the force coefficients acting on the unit length bridge deck

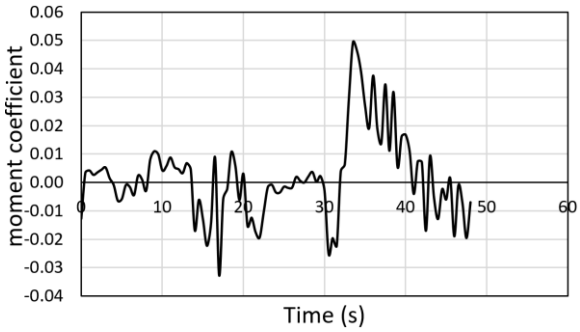

a) moment coefficient about X axis

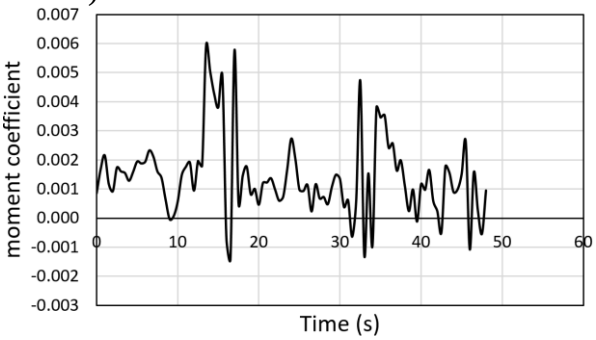

b) moment coefficient about Y axis

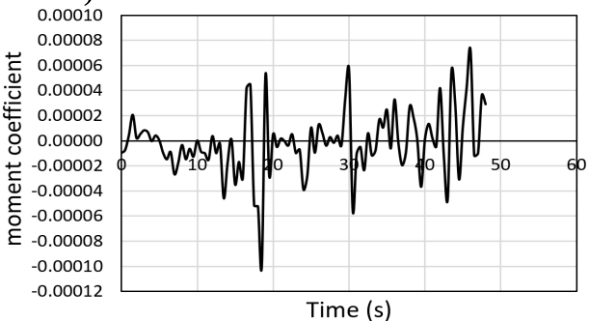

c) moment coefficient about Z axis

Figure 2.14 Time history of the moment coefficients acting on the unit length bridge deck

Chapter 3 Wind Effects of Equivalent Straight-line Winds on Bridges and Its Comparison with Tornadic Wind Effects

Since the current wind design in AASHTO is based on straight-line winds, an equivalent straight-line wind field is established to obtain the wind effects induced by straight-line winds. By comparing the wind effects induced by tornadic winds and its equivalent straight-line winds, the coefficients in the wind pressure equation (in AASHTO) can be modified to calculate the wind pressure induced by tornadoes. In this chapter, the equivalent straight-line wind field is simulated. To study the wind effects of straight-line winds on bridges, the bridge is placed in the equivalent straight-line wind field (see fig. 3.1). The dimension of this rectangular computational domain is determined by the approach applied by Franke (2006).

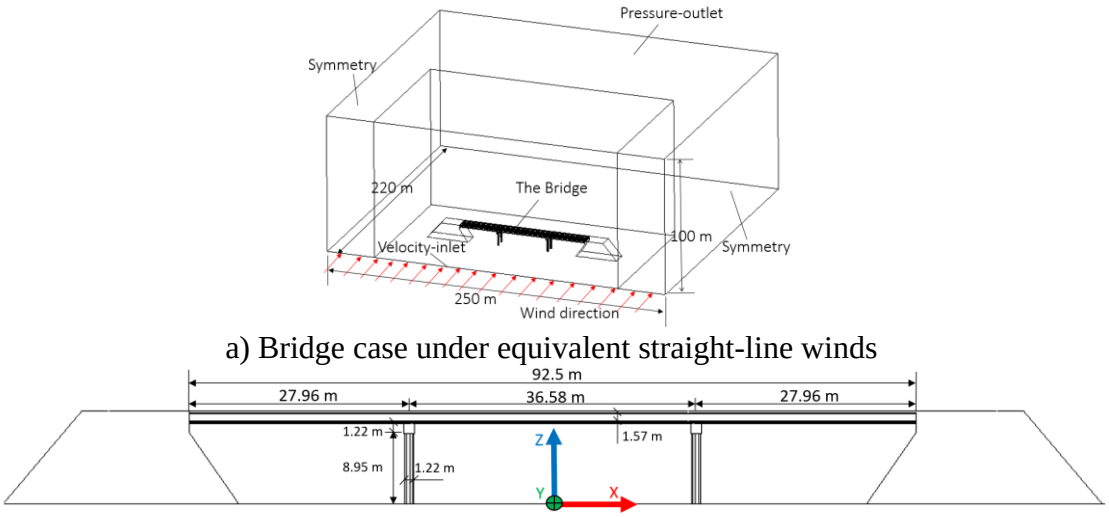

a) Bridge case under equivalent straight-line winds

b) the dimentions of the bridge

Figure 3.1 Computational domains for simulated cases

3.1 Simulation Setup

To simulate the equivalent straight-line winds, the velocity-inlet and pressure-outlet boundaries are 5H and 15H away from the bridge respectively according to Frank (2006), where

H is the height of the bridge. The blockage ratio is below 3%. The velocity input is based on a power-law profile and 0.14 is taken as the exponent, as shown in equation 4.1, which is to simulate the urban/suburban areas. The maximum resultant velocity (the resultant velocity of tangential and radial velocities) at a certain height (H_r= 10.5 m) is 79.9 m/s in the tornadic wind field. Therefore, the velocity profile applied to velocity input is expressed as below

$$V_s = 79.9(Z/H_r)^{0.14} \tag{3.1}$$

where V_s denotes the velocity at different heights; H_r denotes the reference height (H_r= 10.5 m) and Z denotes the height above ground.

3.2 Comparison of the peak pressure on bridge surface induced by tornadic winds and the equivalent straight-line winds

Figure 3.2 presents the streamlines on a horizontal plane of the equivalent straight-line wind field. It shows that two large vortices occur behind the two bridge abutments, which is because the abutments are bluff bodies and will significantly disturb the wind flow on the leeward side. Figure 3.3 presents the time-averaged pressure distribution on bridge surface under the equivalent straight-line winds. It shows that the maximum positive pressure coefficient occurs on the windward wall; and the maximum negative pressure coefficient occurs on the deck instead of the sides of piers. By comparing with the wind pressure induced by tornadic winds (from last chapter) and the equivalent straight-line winds, the maximum positive pressure coefficient occurs under tornadic winds (1.4), which is 17% higher than that induced by the equivalent straight-line winds (1.16); the maximum negative pressure coefficient under tornadic

winds (1.98) is 14% higher than that under straight-line winds (1.71). This infers that the more unfavorable loading condition occurs under tornadic winds.

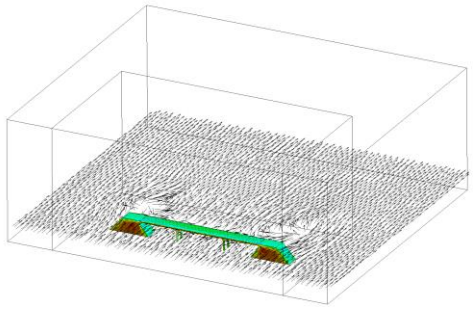

Figure 3.2 Streamlines on a horizaontal plane in the equivalent straight-line wind fields

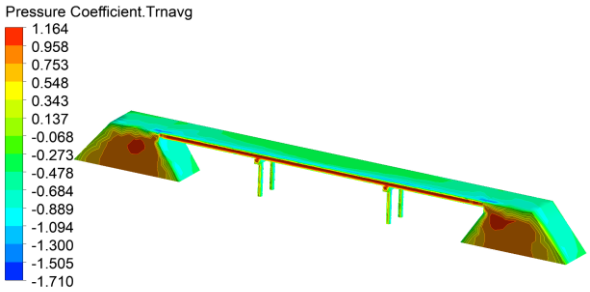

Figure 3.3 Pressure distribution on bridge surface induced by the equivalent straight-line winds

3.3 Comparison of the force and moment coefficients acting on the entire bridge under tornadic winds and under the equivalent straight-line winds

The force coefficients acting on the entire bridge under tornadic winds and under the equivalent straight-line winds are abstracted (see figs. 3.4 and 3.5) and compared in this section. As shown in figure 3.1b), the X direction is along the longitudinal direction of the bridge, the Y direction is perpendicular to the longitudinal direction of the bridge, and the Z direction is the vertical direction. By comparing figures 3.4 and 3.5, the maximum force coefficient in the X direction induced by tornadic winds is 0.8 (see fig. 3.4a)). which is 10 times greater than that induced by the equivalent straight-line winds (0.08, as shown in fig. 3.5a)). In the Z direction, the

maximum force coefficient induced by tornadic winds is 0.62 (see fig. 3.4c)) which is 2.3 times greater than that induced by the equivalent straight-line winds (0.27, as shown in fig. 3.5c)). In the Y direction, the peak value of force coefficient induced by the equivalent straight-line winds (1.33, as shown in fig. 3.5b)) is 1.1 times greater than that induced by tornadic winds (1.2, as shown in fig. 3.4b)). The time history of the force coefficients induced by tornadic winds exhibit two peak values, when t=14s and 34s, which are the time instants when the bridge passes the core radius of the tornado sequentially. From figure 3.5, the force coefficient induced by the equivalent straight-line winds fluctuates in a small range.

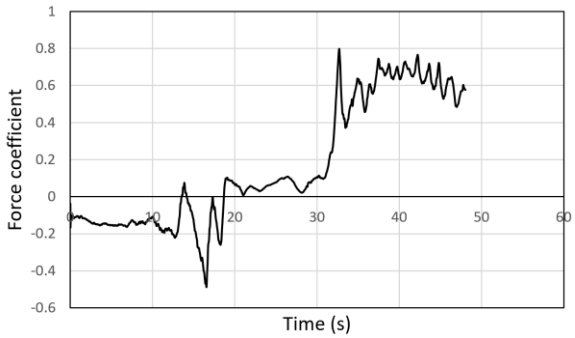

a) Force coefficient in X direction

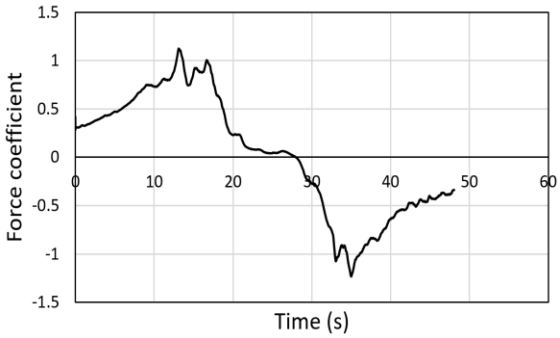

b) Force coefficient in Y direction

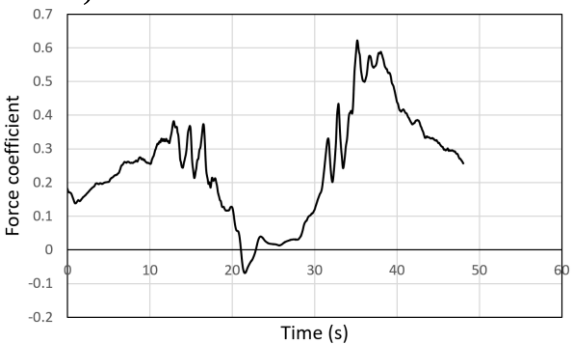

c) Force coefficient in Z direction

Figure 3.4 Time history of force coefficient acting on the bridge under tornadic winds

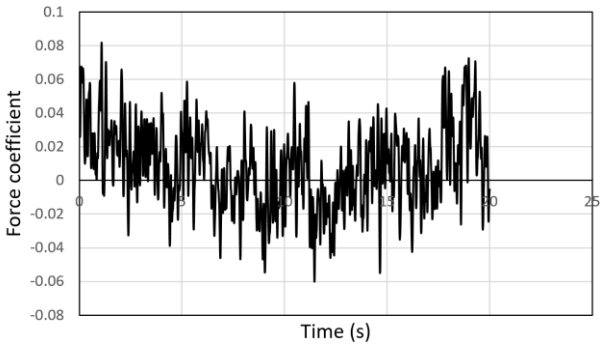

a) Force coefficient in X direction

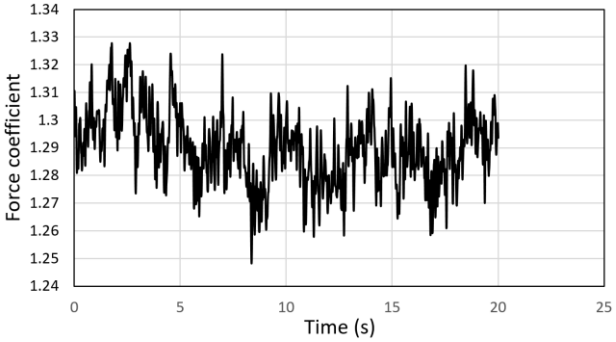

b) Force coefficient in Y direction

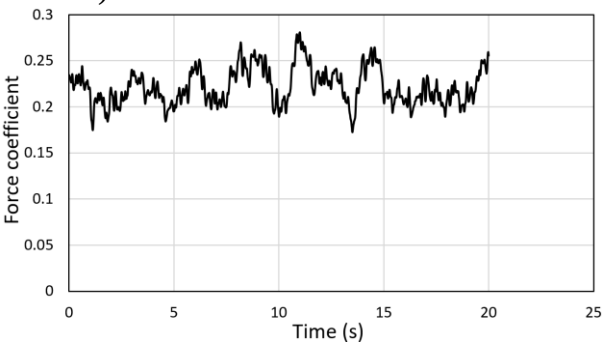

c) Force coefficient in Z direction

Figure 3.5 Time history of force coefficient acting on the bridge under the equivalent straight-line winds

The moment coefficients under the two different types of winds are extracted and presented in figures 3.6 and 3.7. The maximum moment coefficients about the X axis under tornadic winds (5, as shown in fig. 16a)) is 3 times greater than that under the equivalent straight-line winds (1.65, as shown in fig. 17a)). The maximum moment coefficient about the Y axis induced by tornadic winds (0.59, as shown in fig. 16b)) is 4.2 times greater than that

induced by the equivalent straight-line winds (0.14, as shown in fig. 17b)). The maximum moment coefficient about the Z axis induced by tornadic winds (0.032, as shown in fig. 16c)) is 12.8 times greater than that induced by the equivalent straight line winds (0.0025, as shown in fig. 17c)), although both of them are small. The two peak values in the moment time history induced by tornadic winds are associated with the time instants when the bridge passes the two core radii of the tornado sequentially.

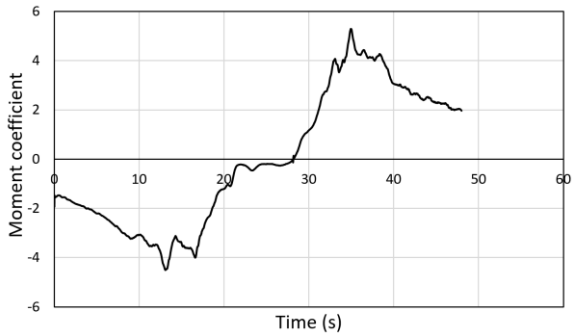

a) Moment coefficient about the X axis

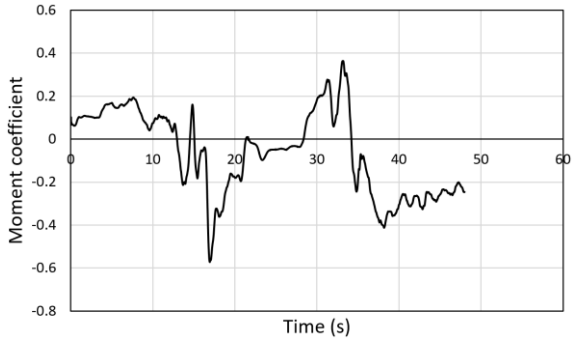

b) Moment coefficient about the Y axis

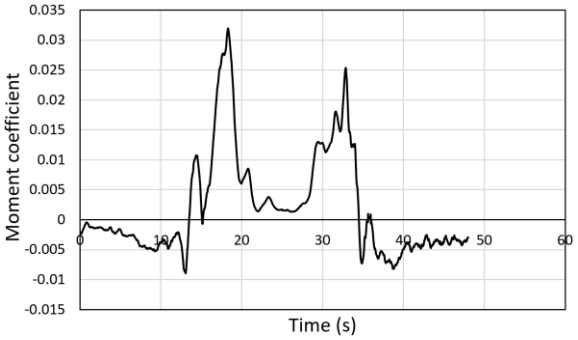

c) Moment coefficient about the Z axis

Figure 3.6 Time history of moment coefficients acting on the bridge under tornadic winds

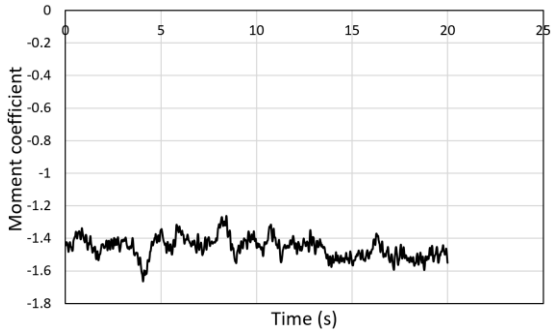

a) Moment coefficient about the X axis

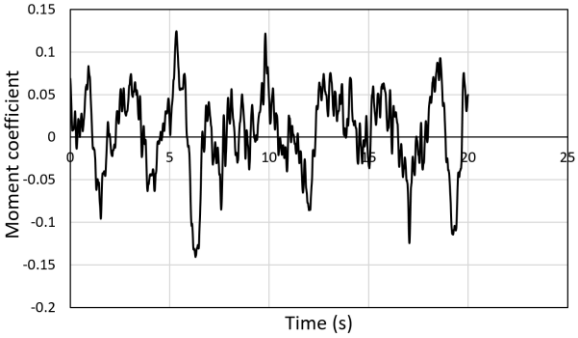

b) Moment coefficient about the Y axis

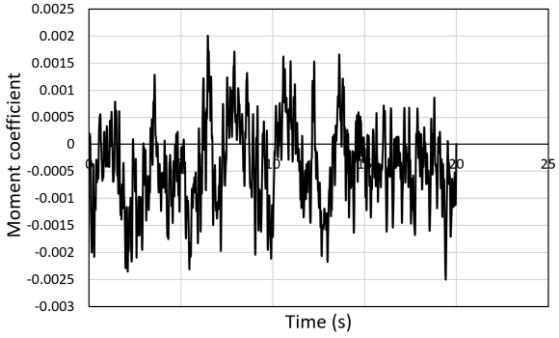

c) Moment coefficient about the Z axis

Figure 3.7 Time history of moment coefficient acting on the bridge under the equivalent straight-line winds

Chapter 4 Modification of the Wind Pressure Equation in AASHTO

The current design of bridges under wind loads is governed by the AASHTO Bridge Design Specifications (American Association of State Highway and Transportation Officials 2017). From this standard, the design wind pressure P_D is computed as

$$P_D = P_B \frac{V_{DZ}^2}{V_B^2} = P_B \frac{V_{DZ}^2}{10000} \left(\frac{kip}{ft^2}\right) \tag{4.1}$$

where the base wind pressure P_B = 0.05 ksf, V_B = 100 mph, and V_{DZ} is the design velocity at a particular elevation.

Equation 4.1 is the wind pressure induced by straight-line winds. Based on the research results obtained from previous chapters, the wind effects of tornadoes are completely different from those induced by straight-line winds, and thus cannot directly use equation 4.1 to calculate the wind pressure induced by tornadoes.

In fact, tornadic wind loads have not been considered as a design load in the latest version of the AASHTO Bridge Design Specifications (the 8th Edition, published in 2017). To enhance the safety of bridges under tornadoes, it is necessary to update the current wind design specifications in AASHTO. The method used in this study is to apply the same V_{DZ} (79.9 m/s at 10.5 m height) under both of the tornadic winds and its equivalent straight-line winds and compare their maximum time-averaged force coefficients on the bridge. Since the force is calculated from the pressure acting on the whole bridge, the comparison between the force coefficients can reflect the relationship between the pressure on the bridge under tornadic winds and its equivalent straight-line winds.

To find out the relationship between the wind effects caused by tornadic winds and its equivalent straight-line winds and obtain the amplification coefficient to modify the wind pressure equation, the time-averaged force coefficients acting on the entire bridge under tornadic winds and under the equivalent straight-line winds are abstracted (see figs. 4.1 and 4.2). As shown in figure 3.1b), the X direction is along the longitudinal direction of the bridge, the Y direction is perpendicular to the longitudinal direction of the bridge on the horizontal plane, and the Z direction is the vertical direction. The time history of the time-averaged force coefficient acting on the bridge under tornadic winds shows the typical trend of the wind effects caused by tornados. That is, two peak values are observed around 14 and 34 seconds, which are the time instants that bridge passes the two core radii of the tornado sequentially. However, under the equivalent straight-line winds, the time history of the time-averaged force coefficients acting on the bridge are relatively stable, although fluctuations do occur.

By comparing the results from figures 4.1 and 4.2, the maximum force coefficient in the X direction induced by the tornadic winds is 0.7 (see fig. 4.1a)), which is 26 times greater than that induced by the equivalent straight-line winds (0.027, as shown in fig. 4.2a)). The time-averaged force coefficient in the X direction is very small under straight-line winds since the straight-line winds blow along the Y direction which lead to tiny force in the X direction. So, the comparison of time averaged force coefficient in X direction is not a reasonable reference. In the Y direction, the peak value of the time-averaged force coefficient induced by the tornadic winds (1.15, as shown in fig. 4.1b)) is 1.13 times smaller than that induced by the equivalent straight-line winds (1.3, as shown in fig. 4.2b)). In the Z direction, the maximum averaged force coefficient induced by the tornadic winds is 0.57 (see fig. 4.1c)), which is 2.42 times greater than that induced by the equivalent straight-line winds (0.236, as shown in fig. 4.2c)). Thus, the

highest ratio between the maximum time-averaged force coefficient under tornadic winds and its equivalent straight-line winds is 2.42 in the Z direction, which is because of the higher suction caused by the atmospheric pressure drop in the tornado. Hence, the current wind pressure equation can be modified by introducing a coefficient, as shown below:

$$P_D = 2.42P_B \frac{V_{DZ}^2}{V_B^2} = 2.42P_B \frac{V_{DZ}^2}{10000} \left(\frac{kip}{ft^2}\right) \quad (4.2)$$

where P_B = 0.05 ksf, V_B = 100 mph, and V_{DZ} is the design velocity at a particular elevation.

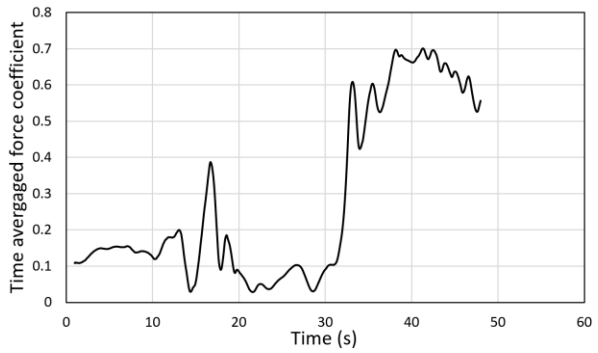

a) Force coefficient in X direction

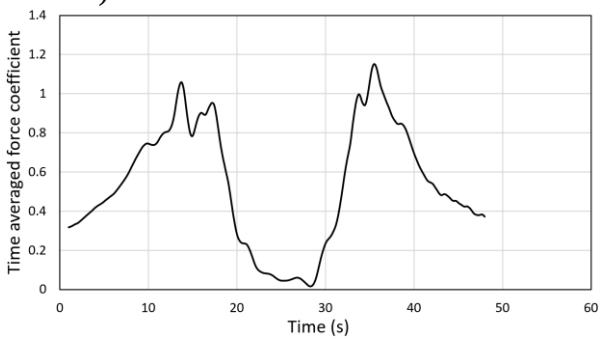

a) Force coefficient in Y direction

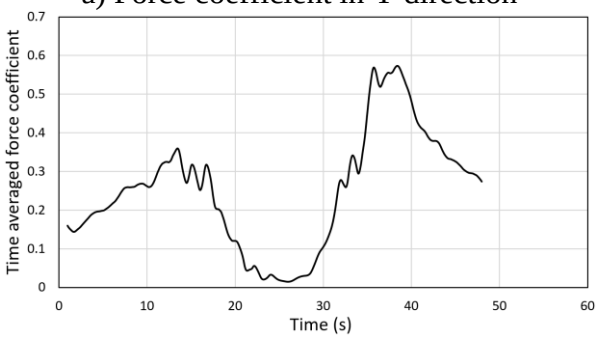

a) Force coefficient in Z direction

Figure 4.1 Time history of the time-averaged force coefficient acting on the bridge under tornadic winds

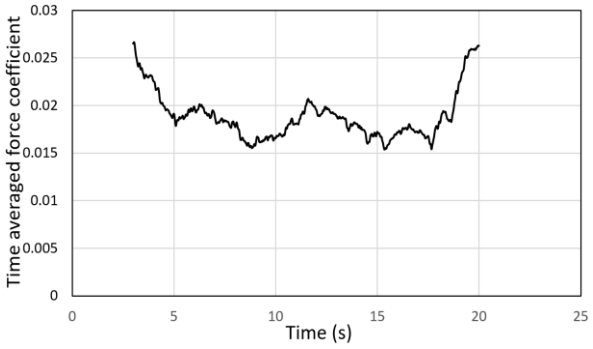

a) Force coefficient in X direction

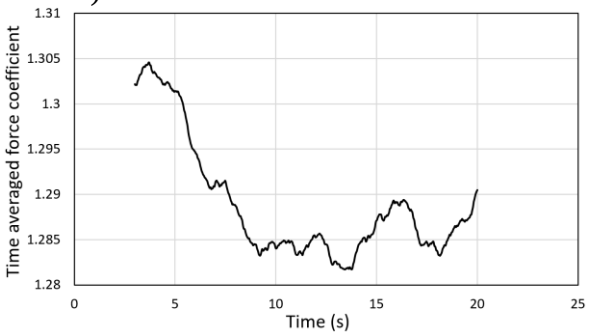

a) Force coefficient in Y direction

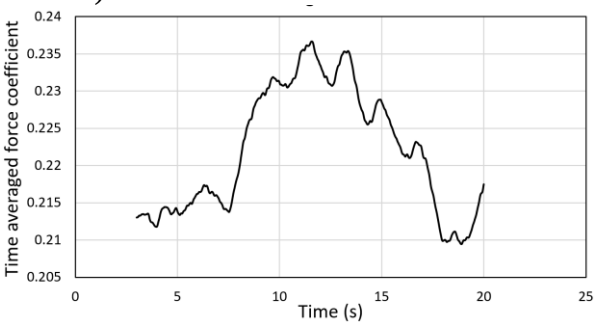

a) Force coefficient in Z direction

Figure 4.2 Time history of the time-averaged force coefficient acting on the bridge under the equivalent straight-line winds

Chapter 5 Conclusions and Future Work

This research is to characterize the wind effects of tornadoes on bridges using computational fluid dynamics (CFD) simulations, and to update the equations for calculating the design wind pressure towards a tornado-resistant design.

The research outcomes include: 1) A high-fidelity numerical model to obtain the wind pressure distribution on girder bridges induced by tornadoes; 2) A modified equation for calculating wind pressure towards a tornado-resistant design for bridges. The obtained design tornadic wind loads can be used to evaluate the vulnerability of existing bridges, to develop a reinforcing strategy (reinforcing connections between structural components) for existing bridges to achieve a continuous load path. This research will eventually advance the design theory of highway bridges based on the in-depth understanding of tornadic wind effects.

This project is Phase 1 of this research, which is to characterize the tornadic wind effects on those bridges that do not normally experience large deformation and vibration during strong winds. That is, the bridge will be assumed to be rigid in the computational domain and the wind pressure on the bridge is determined without the consideration of the wind-bridge interaction, which is suitable for short-span or middle-span bridges. Phase 2 of this research is to characterize the wind effects induced by tornadoes on those bridges whose deformation and vibration are significant under strong winds. In this case, the wind-bridge interaction will be simulated. This is suitable for long-span bridges and will be conducted in the next project.

References

1. Lott, N., Smith, A., Houston, T., Shein, K., & Crouch, J. (2012). Billion dollar US weather/climate disasters, 1980-2011. *National Climatic Data Center (http: //www. ncdc. noaa. gov/oa/reports/billionz. html).*

2. FEMA (2012). Spring 2011 tornadoes: April 25–28 and May 22, Building performance observations, recommendations, and technical guidance. *Mitigation Assessment Team Report*, FEMA P-908, 512. (http:// www.fema.gov/library/viewRecord.do?)

3. Leech, T.G., McHugh, J.D., & Dicarlantonio, G. (2005). Lessons from the Kinzua. Civil Engineering, 56-61.

4. Minor, J.E., McDonald, J.R. and Mehta, K.C., 1977. The tornado: An engineering-oriented perspective. NASA STI/Recon Technical Report N, 78.

5. Mishra, A. R., James, D. L., & Letchford, C. W. (2008). Physical simulation of a single-celled tornado-like vortex, Part A: Flow field characterization. *Journal of Wind Engineering and Industrial Aerodynamics*, *96*(8), 1243-1257.

6. Refan, M. (2014). Physical simulation of tornado-like vortices (Doctoral dissertation, The University of Western Ontario).

7. Haan, F. L., Sarkar, P. P., & Gallus, W. A. (2008). Design, construction and performance of a large tornado simulator for wind engineering applications. *Engineering Structures*, *30*(4), 1146-1159.

8. Haan Jr, F. L., Balaramudu, V. K., & Sarkar, P. P. (2009). Tornado-induced wind loads on a low-rise building. *Journal of structural engineering*, *136*(1), 106-116.

9. Chang, C. C. (1971). Tornado wind effects on buildings and structures with laboratory simulation. In *Proceedings of the Third International Conference on Wind Effects on Buildings and Structures* (pp. 231-240).

10. Bienkiewicz, B., & Dudhia, P. (1993, June). Physical modeling of tornado-like flow and tornado effects on building loading. In *Proceeding 7th US National Conference on Wind Engineering* (pp. 95-106).

11. Fouts, J. L., James, D. L., & Letchford, C. W. (2003). Pressure distribution on a cubical model in tornado-like flow. In *11th International Conference on Wind Engineering* (Vol. 10, p. x).

12. Rajasekharan, S. G., Matsui, M., & Tamura, Y. (2013). Characteristics of internal pressures and net local roof wind forces on a building exposed to a tornado-like vortex. *Journal of Wind Engineering and Industrial Aerodynamics*, *112*, 52-57.

13. Sabareesh, G. R., Matsui, M., & Tamura, Y. (2013). Ground roughness effects on internal pressure characteristics for buildings exposed to tornado-like flow. *Journal of Wind Engineering and Industrial Aerodynamics*, *122*, 113-117.

14. Kuai, L., Haan Jr, F. L., Gallus Jr, W. A., & Sarkar, P. P. (2008). CFD simulations of the flow field of a laboratory-simulated tornado for parameter sensitivity studies and comparison with field measurements. *Wind and Structures*, 11(2), 75-96.

15. Ishihara, T., Oh, S., & Tokuyama, Y. (2011). Numerical study on flow fields of tornado-like vortices using the LES turbulence model. *Journal of Wind Engineering and Industrial Aerodynamics*, 99(4), 239-248.

16. Yuan, F., Yan, G., Honerkamp, R. and Isaac, K.M. (2017), "Numerical Simulation of Laboratory Tornado Simulator that can Produce Translating Tornadoes," *Journal of Wind Engineering and Industrial Aerodynamics*. Under review.

17. Hangan, H., & Kim, J. D. (2008). Swirl ratio effects on tornado vortices in relation to the Fujita scale. *Wind and Structures*, 11(4), 291-302.

18. Li, Z., Honerkamp, R., Yan, G., & Feng, R. (2020). Influence of a community of buildings on tornadic wind fields. *Wind and Structures*, *30*(2), 165-180.